Frontiers in Bioscience Landmark

Front. Biosci. (Landmark Ed) **2026**; 31(1): 46975
https://doi.org/10.31083/FBL46975

Original Research

Multimodal Enhancement of Colonic Motility by Acupuncture at ST36 is Mediated by TRPV1$^+$ Cutaneous Sensory Fibers

Nan Zhang[1,†], Huilin Chen[1,†], Xinyan Gao[1], Sha Li[2], Xia Li[1], Wang Li[2], Kun Liu[1], Shuya Wang[1,*], Bing Zhu[1,*]

[1]Institute of Acupuncture and Moxibustion, China Academy of Chinese Medical Sciences, 100700 Beijing, China
[2]Institute of Basic Theory for Chinese Medicine, China Academy of Chinese Medical Sciences, 100700 Beijing, China
*Correspondence: wangshuya@mail.cintcm.ac.cn (Shuya Wang); zhubing@mail.cintcm.ac.cn (Bing Zhu)
[†]These authors contributed equally.
Academic Editor: Graham Pawelec
Submitted: 27 September 2025 Revised: 22 December 2025 Accepted: 31 December 2025 Published: 21 January 2026

Abstract

Background: Acupuncture has been shown to promote gastrointestinal motility. This study explores whether cutaneous transient receptor potential vanilloid 1 (TRPV1)$^+$ fibers at Zusanli (ST36) acupoint can mediate the multimodal effects of acupuncture on colorectal motility, as well as examining their mechanistic role. **Methods**: C57BL/6 mice were subjected to electroacupuncture (EA), manual acupuncture (MA), 46 °C thermal stimulation, and 1% capsaicin at the ST36 acupoint. Colon motility was quantified via the area under the curve (AUC) and contraction amplitude. Immunofluorescent co-localization of TRPV1 with CGRP, NF200, peripherin, and tyrosine hydroxylase (TH) was conducted in *TrpV1*^{Cre} mice to determine neural phenotypic subtypes. Furthermore, *TrpV1*$^{ChR2\text{-}eYFP}$ and *TrpV1*$^{NpHR\text{-}eYFP}$ transgenic mice that underwent optogenetic activation or silencing of local TRPV1$^+$ fibers at ST36 were evaluated for acupuncture-like stimulation effects on colorectal AUC and amplitude. **Results**: All applied stimuli in C57BL/6 mice significantly increased colorectal motility parameters (AUC and amplitude, $p < 0.05$) compared to baseline. TRPV1$^+$ somatosensory neurons in the dorsal root ganglion (DRG) predominantly co-expressed with peripherin (46.76%) and CGRP (27%), which are markers of unmyelinated peptidergic fibers, but rarely with NF200 (6%) or TH (< 1%). Optogenetic activation (30 mW blue light) of TRPV1$^+$ fibers in *TrpV1*$^{ChR2\text{-}eYFP}$ mice mimicked acupuncture-like stimuli, with significantly enhanced colorectal AUC and amplitude ($p < 0.05$). In contrast, optogenetic silencing of TRPV1$^+$ fibers with yellow light abolished acupuncture-like stimulation of colorectal motility in *TrpV1*$^{NpHR\text{-}eYFP}$ mice ($p <$ 0.05). **Conclusion**: Through the use of spatiotemporally precise optogenetic control, our study revealed that TRPV1$^+$ sensory fibers at ST36 are the major convergent pathway for multimodal (electrical/mechanical/thermal/chemical) enhancement of colorectal motility by acupuncture.

Keywords: dorsal root ganglion; TRPV1; colon; acupuncture

1. Introduction

Acupuncture represents a somatosensory neuromodulatory intervention and exerts its therapeutic effects through mechanotransduction in cutaneous and subcutaneous tissues. This is mediated by peripheral primary sensory afferent fibers. Acupuncture is also considered a mainstream therapeutic modality for functional gastrointestinal disorders (FGIDs), with many randomized clinical trials (RCTs) published in high-impact journals demonstrating statistically significant improvements in global symptom relief [1–5]. As one kind of somatic stimulation, acupuncture can transmit stimuli through the dorsal root ganglion (DRG) and spinal cord level to achieve an analgesic effect on visceral pain and modulate gastrointestinal motility [6–9]. However, it remains unclear which specific subtypes of DRG neurons mediate the effects of acupuncture.

DRG serves as a critical relay station for peripheral-to-central nervous system signaling [10]. Emerging evidence highlights the functional specificity of small-to-medium diameter DRG neurons in mediating somatosensory stimulation-induced modulation of visceral homeostasis through somatovisceral regulatory pathways, particularly through highly-expressed transient receptor potential vanilloid 1 (TRPV1) receptors [10,11]. Indeed, TRPV1 is anatomically positioned as a core signaling mediator in acupuncture-induced somato-visceral integration, localizing to cutaneous nociceptive terminals, small-to-medium diameter DRG neurons, spinal cord dorsal horn nuclei, and visceral afferent networks [12]. *In vivo* constitutive TRPV1-deficient models exhibit attenuated acupuncture-mediated gastric modulation [13,14], while electrophysiological evidence shows that TRPV1-dependent colorectal stimulation in Vil-ChR2 mice elicits behavioral responses that was similar to that seen with balloon distension of the colon [15]. Collectively, this suggests that TRPV1-expressing, small-to-medium DRG neurons are the leading candidate subtype mediating the effects of acupuncture on visceral function.

Despite this compelling association, the proportional mechanistic contribution of TRPV1 specifically within

acupuncture-mediated visceromotor regulation remains unknown. This knowledge gap is compounded by the systemic pleiotropy of TRPV1 expression across multiple physiological axes, thereby complicating interpretation in traditional global knockout models. To address this limitation, the present study employed optogenetic interrogation for spatiotemporally precise activation and inhibition of $TRPV1^{+}$ neural circuits at the ST36 (Zusanli) acupoint. This targeted strategy circumvents the interpretative limitations inherent to global knockout models. Moreover, it enables mechanistic dissection of TRPV1-dependent gut-brain signaling in acupuncture-evoked colorectal motility regulation, as well as quantitative determination of its modality-specific contributions to colorectal neuromodulation.

2. Materials and Methods

2.1 Animals

A total of 21 adult mice (22–25 g body weight) were used in this study, comprising 6 C57BL/6 wild-type mice, 2 $TrpV1^{Cre}$ mice, 8 $TrpV1^{ChR2\text{-}eYFP}$ mice (expressing ChR2-EYFP), and 5 $TrpV1^{NpHR\text{-}eYFP}$ mice (expressing NpHR3.0-EYFP). The sex of the animals was not distinguished in the experimental design. C57BL/6 mice (22–25 g) were obtained from SPF Biotechnology Co., Ltd. (Beijing, China). The $TrpV1^{Cre}$ mouse line (Stock No. 017769) was generously provided by Dr. Shenbin Liu's laboratory at Fudan University. Optogenetic mouse lines, including ChR2 (Ai32; Stock No. 024109) and NpHR (Ai39; Stock No. 014539), were acquired from The Jackson Laboratory (Bar Harbor, ME, USA). Transgenic $TrpV1^{ChR2\text{-}eYFP}$ and $TrpV1^{NpHR\text{-}eYFP}$ mice (22–25 g) were generated and maintained by Shanghai Model Organisms Center, Inc. (Shanghai, China).

All animals were housed in standard polycarbonate cages (maximum 5 mice per cage) with *ad libitum* access to autoclaved water and standard rodent chow. The vivarium was maintained at 22 ± 1 °C, 50 ± 5% relative humidity, and a 12:12 h light-dark cycle (lights on at 07:00). All experimental procedures were conducted in accordance with the National Institutes of Health Guide for the Care and Use of Laboratory Animals and were approved by the Experimental Animal Ethics Committee of the Chinese Medical Sciences (No. D2024-01-26-07). Procedures were performed under isoflurane anesthesia (induction: 4%, maintenance: 1.5–2% in 100% O_2), with body temperature maintained at 37 ± 0.5 °C using a feedback-controlled heating pad. Euthanasia was performed by isoflurane (5%) followed by cervical dislocation.

2.2 Colorectal Motility Recording Protocol

The fabricated polyethylene balloon catheters used here were described previously [13]. Catheter integrity was validated prior to experimentation via underwater pressure testing (1 mL syringe inflation) to confirm the balloon membrane integrity and leak-proof tubing connections. Following 4-h fasting (*ad libitum* water access), mice were anesthetized with 4% isoflurane in oxygen for induction and 2% isoflurane via nose cone for maintenance. The lubricated balloons were inserted 2 cm beyond the anal verge.

Following surgical preparation, a three-way stopcock was connected to a calibrated pressure transducer (Biopac Systems) pre-filled with distilled, deionized water. The system was meticulously purged of air bubbles to ensure signal fidelity, and the recording apparatus was then initialized and calibrated. This comprised a NeuroLog NL108A amplifier (Digitimer Ltd., Letchworth, UK), Micro1401 data acquisition interface (Cambridge Electronic Design, Cambridge, UK), and Spike2 software (v7.03, Cambridge Electronic Design, Cambridge, UK).

The stopcock configuration was adjusted to establish atmospheric pressure equilibration within the balloon system. Baseline calibration was performed to establish a 0 cmH_2O reference. A precise volume of distilled water (50–100 µL) was injected into the balloon using a calibrated microsyringe (Hamilton Company, Bonaduz, Switzerland). The spherical water-filled balloon, positioned within the colorectal lumen, transduced intraluminal pressure changes, which were transmitted hydrostatically through the polyethylene catheter to the pressure transducer. The analog pressure signal was amplified (NeuroLog NL108A) and digitized (Micro1401) for acquisition. Real-time signal visualization and recording were performed using Spike2 (v7.03, Cambridge Electronic Design Limited, British) with appropriate filtering.

Following stabilization of the colorectal motility patterns (typically 15–30 minutes post-surgical preparation), baseline recordings were acquired for 1 minute prior to stimulation. Each stimulation protocol was administered for precisely 1 minute, followed by a minimum 5-minute washout period to allow complete recovery of motility parameters to baseline levels, as confirmed by real-time monitoring of pressure traces. This inter-stimulus interval was maintained to prevent carryover effects between experimental conditions. Comparative waveform analysis between pre-stimulation baseline and stimulation periods was performed using two key parameters: Area Under Curve (AUC), and Contractile Amplitude. AUC, pressure-time integral, represents the total propulsive effort ($cmH_2O{\cdot}s$), while amplitude (Δp = max–min) reflects instantaneous neuromuscular drive (cmH_2O).

2.3 Acupuncture-Like Intervention Protocol

The ST36 acupoint was localized according to standardized anatomical landmarks described in the Experimental Acupuncture reference text. It was identified as 3 mm lateral to the tibial crest at the knee joint level, corresponding to the classical anatomical position in murine models. Stimulation duration was maintained for 1 minute.

EA was administered using acupuncture needles connected to a Constant Current Isolated Stimulator (DS3; Digi-timer Ltd., Welwyn Garden City, UK). Stimulation parameters were set at 1 mA intensity, 10 Hz frequency, and 1 ms pulse width. The needle was inserted vertically to a depth of 5 mm at the ST36 acupoint. Manual Acupuncture (MA) was performed by a single trained practitioner to ensure consistency. Following vertical needle insertion, manual stimulation was applied using a standardized technique involving rapid bidirectional rotation (180° clockwise and counterclockwise) at a 2 Hz frequency for 1 minute. A calibrated temperature probe was heated to 47 $\pm$ 0.5 °C using a precision circulating water bath (set at 48 °C to maintain thermal stability). Following depilation, the probe was applied to the ST36 acupoint with consistent pressure for 1 minute, ensuring maintenance of the target temperature (46 °C) throughout the stimulation period. A capsaicin (CAP) solution was prepared in 99.5% ethanol (1% w/v). Sterile cotton applicators (0.2 mm diameter) were saturated with the solution and applied to the depilated ST36 acupoint for 1 minute, ensuring complete contact with the skin surface.

As illustrated in Fig. 1A, four different types of stimulation were applied sequentially to the ST36 acupoint of C57BL/6 mice: EA, MA, 46 °C, and CAP. The waveforms were subsequently compared before and during the stimulation.

2.4 Optogenetic Stimuli

Light (473/593 nm) for stimulation was delivered through a 200 µm diameter optical fiber (RWD, R-FC-L-N2-200-L1) positioned perpendicular to the skin and affixed tightly against it. The fiber tip was placed directly above the ST36 acupoint. Prior to each experiment, laser power output from the fiber optic cable was measured using a photometer (PM100D, Thor Labs, Newton, NJ, USA).

The optogenetic activation protocols shown in Fig. 3A employed identical motility recording and analysis pipelines as those established in prior experiments, with light parameters optimized to achieve suprathreshold TRPV1$^+$ fiber activation (473 nm, 30 mW, 10 Hz).

For yellow light inhibition stimulation, after the colorectal motility recordings in mice had stabilized, a 1-minute recording segment was selected as the baseline for comparison. This was followed by a 1-minute EA (1 mA, 10 Hz) stimulation. Once the colorectal motility trace returned to a stable state, another 1-minute baseline was selected. Yellow light stimulation (20 mW, 10 Hz) was then applied for 30 seconds in advance, followed by a combined stimulation of yellow light (20 mW, 10 Hz) and EA (1 mA, 10 Hz) for 1 minute. The process was repeated with increasing intensities of yellow light, as shown in Fig. 6A. Changes in the AUC and amplitude of colorectal motility induced by EA alone and by the combination of yellow light and EA were compared. As shown in Fig. 7A, after determining the effective intensity of yellow light (30 mW, 10 Hz), different peripheral acupuncture-like stimuli were sequentially applied, with the same operational procedures and statistical parameters as described previously.

2.5 Immunofluorescence Staining

After recording of colorectal motility, *TrpV1*$^{ChR2\text{-}eYFP}$ and *TrpV1*$^{NpHR\text{-}eYFP}$ mice were weighed and anesthetized with 1.25% tribromoethanol (Avertin; 2 mL/100 g body weight, i.p.). *TrpV1*^{Cre} mice, which did not undergo motility recording, were weighed and anesthetized directly (Avertin; 2 mL/100 g body weight, i.p.). Following depilation of the ST36 acupoint region using electric clippers, thoracotomy was performed to expose the cardiac apex. Systemic perfusion was initiated with 40 mL of ice-cold phosphate-buffered saline (PBS; 0.9%, pH 7.4) followed by 40 mL of freshly prepared 4% paraformaldehyde (PFA) in 0.1 M phosphate buffer (PB; pH 7.4), delivered at a rate of 5 mL/min using a peristaltic pump. Following perfusion, bilateral DRG from lumbosacral (L6–S2) segments were dissected and post-fixed in 4% PFA for 3 h at 4 °C. Tissues were then cryoprotected through sequential sucrose gradients (15% and 30% in 0.1 M PB) at 4 °C until equilibrium (typically 24–48 h), as determined by tissue sedimentation. Cryoprotected samples were stored in 30% sucrose solution at 4 °C until further processing.

Following complete cryoprotection, tissue samples were embedded in optimal cutting temperature (OCT) compound (Epredia Richard-Allan NEG 50, Kalamazoo, MI, USA) and rapidly frozen on a cryostat microtome freezing chamber (Leica CM1950, Wetzlar, Germany). Serial coronal sections (20 µm thickness) were obtained using a cryostat microtome maintained at –20 °C. Sections were systematically collected and mounted onto positively charged glass slides (Superfrost Plus, Thermo Fisher Scientific, Waltham, MA, USA). To ensure tissue integrity and minimize freeze-thaw artifacts, sections were air-dried for 30 minutes at room temperature.

Tissue sections were rehydrated in 0.1 M PB (pH 7.4) for 10 minutes to remove residual OCT compound. Non-specific binding sites were blocked with a solution containing 5% normal goat serum (Jackson ImmunoResearch, West Grove, CA, USA), 0.5% Triton X-100 (Sigma-Aldrich, Saint Louis, MO, USA), and 0.1 M PB for 1 h at room temperature (22 $\pm$ 1 °C).

The following primary antibodies were diluted in antibody dilution buffer (3% normal goat serum, 0.5% Triton X-100 in 0.1 M PB) and applied to sections: TRPV1 (1:600, GP14100, NEUROM), CGRP (1:1500, 24112, IMMUNOSTAR), NF200 (1:600, Ab207176, Abcam), PER (1:1000, AVES, NEUROM), TH (1:600, ab112, Abcam), and GFP (1:1000, GFP-1010, Aves Labs). Incubation was performed in a humidified chamber at 4 °C for 16–18 h. After three 10-minute washes in 0.1 M PB, the following species-specific secondary antibodies conjugated with Alexa Fluor dyes (Thermo Fisher Scientific, Waltham, MA,

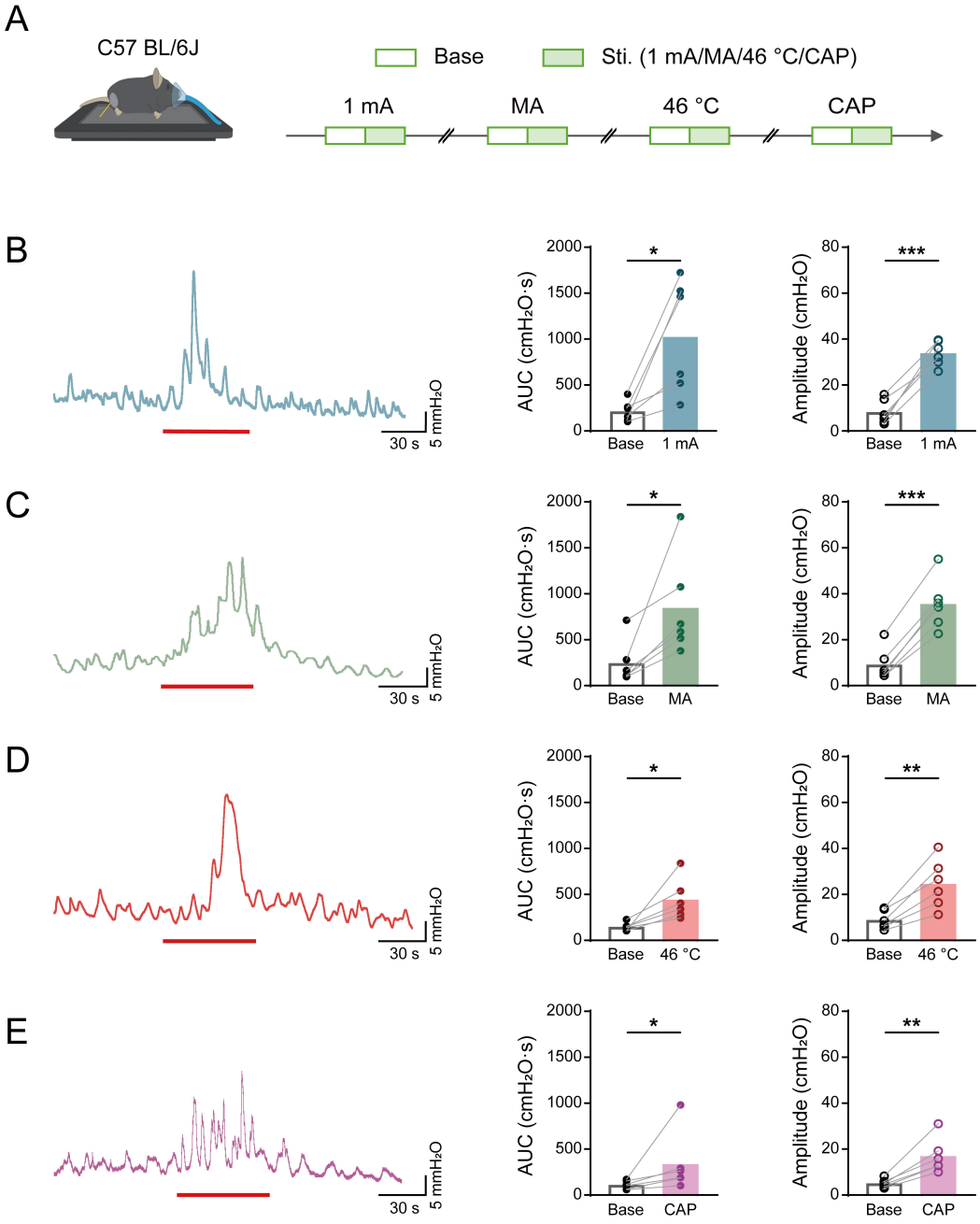

Fig. 1. Effects of diverse acupuncture-like stimuli at ST36 on colorectal motility in C57 mice. (A) Experimental flowchart for acupuncture-like stimulation at ST36 in C57 mice. Mouse image was modified from Heaster TM *et al.* (https://doi.org/10.3389/fbioe.2021.644648). (B–E) Representative example graphs of colorectal motility (left), and statistical graphs of AUC (middle) and amplitude (right) during EA (B), MA (C), 46 °C heat (D), and capsaicin (E) stimulation of C57 mice at ST36. Length of each red trace refers to 1 min. n = 6, *$p < 0.05$, **$p < 0.01$, ***$p < 0.001$ *vs.* base. ST36, Zusanli acupoint; AUC, area under the curve; EA, electroacupuncture; MA, manual acupuncture.

USA) were applied at a 1:500 dilution in antibody dilution buffer and incubated for 2 h at room temperature in darkness: goat anti-guinea pig 594 (A-11076, ThermoFisher, Waltham, MA, USA), goat anti-chicken 488 (A-11039, ThermoFisher), and goat anti-rabbit 488 (A32731, ThermoFisher, Waltham, MA, USA). Following three washes, sections were then coverslipped using anti-fade mounting medium containing 50% glycerol (Vector Laboratories, San Francisco, CA, USA) and sealed with clear nail polish.

Fluorescence imaging was performed using an epifluorescence microscope (Olympus FV1200, Tokyo, Japan) equipped with appropriate filter sets and a confocal laser scanning microscope (Zeiss LSM 880, Oberkochen, Germany) with 20× and 40× objectives. Quantitative analysis

of immunopositive cells was conducted using ImageJ software (v1.53, NIH, Bethesda, MD, USA).

2.6 Statistical Analysis

All statistical analyses were performed using GraphPad Prism software (version 8.0, GraphPad Software Inc., San Diego, CA, USA). Data are expressed as the mean ± standard error of the mean (SEM), unless otherwise specified. Normality of data distribution was assessed using the Shapiro-Wilk test. For normally distributed paired data, parametric analysis was conducted using paired Student's *t*-tests. Non-parametric data were analyzed using Wilcoxon signed-rank tests to evaluate the effects of stimulation on intestinal motility parameters. Multiple group comparisons were performed using one-way analysis of variance (ANOVA) followed by Tukey's post hoc test for normally distributed data, or the Kruskal-Wallis test with Dunn's correction for non-parametric data. The threshold for statistical significance was set at $p < 0.05$. All statistical tests were two-tailed, with adjustment for multiple comparisons where appropriate.

3. Results

3.1 Effects of Different Acupuncture-Like Stimuli at ST36 on Colorectal Motility in C57 Mice

We first systematically characterized the effects of diverse acupuncture-like stimuli modalities on colorectal motility patterns in C57BL/6 mice, focusing on the ST36 acupoint. The stimulation paradigm incorporated four distinct interventions, as illustrated in Fig. 1A.

Quantitative analysis of colorectal motility parameters (Fig. 1B–E) revealed that all stimulation modalities significantly enhanced motor function compared to baseline recordings. Specifically, marked increases were observed in the AUC (EA: from 214.8 ± 45.8 to 1022 ± 251.4, $p = 0.0174$; MA: from 246.5 ± 97.34 to 845.2 ± 220.8, $p = 0.0313$; 46 °C: from 147 ± 18.58 to 441.7 ± 90.22, $p = 0.0313$; CAP: from 111.4 ± 18.66 to 335.7 ± 131.9, $p = 0.0313$), as well as in contraction amplitude (EA: from 8.22 ± 2.19 to 33.83 ± 2.21, $p = 0.0002$; MA: from 9.15 ± 2.84 to 35.54 ± 4.54, $p < 0.0001$; 46 °C: from 8.93 ± 1.65 to 24.58 ± 4.32, $p = 0.0037$; CAP: from 5.11 ± 0.77 to 16.96 ± 3.09, $p = 0.0043$). These findings indicate that multiple forms of acupuncture-like stimuli at ST36 can effectively modulate colorectal motility function in C57BL/6 mice.

3.2 Characterization of TRPV1 in the DRG of $TrpV1^{Cre}$ Mice

In order to demonstrate the effectiveness of the TRPV1 channel in acupuncture-like stimuli, we conducted detailed immunohistochemical characterization of TRPV1-expressing neurons in DRG sections from $TrpV1^{Cre}$ mice, focusing especially on the homosegemental level (L6–S2, Fig. 2). Quantitative analysis demonstrated that TRPV1 predominantly co-localized with markers of unmyelinated peptidergic neurons (CGRP: 27.39 ± 0.11%; PER: 46.76 ± 0.61%), while showing minimal overlap with $NF200^+$ myelinated neurons (6.10 ± 3.23%) and TH^+ sympathetic fibers (<1%). This molecular profiling establishes TRPV1 as a marker of small-diameter, nociceptive neurons, prompting subsequent investigation of its functional involvement in acupuncture-mediated neural modulation.

3.3 Optimal Intensity of Blue Light Stimulation of ST36 to Activate Colorectal Motility in $TrpV1^{ChR2\text{-}eYFP}$ Mice

To determine whether $TRPV1^+$ neurons are the best candidates for acupuncture effects, we generated $TrpV1^{ChR2\text{-}eYFP}$ mice in which cutaneous TRPV1 sensory neurons can be selectively activated with precise temporal and spatial control using an external source of blue light. $TrpV1^{ChR2\text{-}eYFP}$ mice were generated by breeding Ai32 mice [16] with mice expressing Cre recombinase under the control of the TRPV1 promoter [17]. ChR2-expressing neurons in DRG can be visualized using immunofluorescence microscopy based on their expression of eYFP. As expected, $TRPV1^+$ neurons in the DRG of $TrpV1^{ChR2\text{-}eYFP}$ mice co-expressed eYFP (Fig. 3A).

To determine the optimal optical stimulation parameters, we systematically evaluated the intensity of blue light (473 nm) on colorectal motility patterns in $TrpV1^{ChR2\text{-}eYFP}$ transgenic mice using a graded intensity protocol ranging from subthreshold to suprathreshold levels (20–40 mW). As shown in Fig. 3B–D, optical stimulation was achieved at 473 nm with the parameters of 10 Hz frequency, 1 ms pulse width, and 1 min illumination duration. This elicited a significant increase in colorectal motility, as quantified by both AUC and contraction amplitude. Notably, light intensities of 30 mW and 40 mW produced robust and statistically significant responses (AUC: 20 mW, from 189.2 ± 38.44 to 161.6 ± 31.75, $p = 0.0625$; 30 mW, from 178.4 ± 60.43 to 306.2 ± 98.23, $p = 0.0399$; 40 mW, from 100.3 ± 13.62 to 215.4 ± 24.21, $p = 0.0083$. Contraction amplitude: 20 mW, from 6.28 ± 1.53 to 6.63 ± 1.46, $p = 0.8125$; 30 mW, from 8.15 ± 2.66 to 14.2 ± 3.13, $p = 0.0059$; 40 mW, from 4.58 ± 0.72 to 11.02 ± 1.17, $p = 0.0185$). Therefore, 30 mW was selected as the optimal stimulation intensity for subsequent optogenetic manipulations.

3.4 Comparison of the Effects of Blue Light and Acupuncture-Like Stimulation at ST36 on the Regulation of $TrpV1^{ChR2\text{-}eYFP}$ Colorectal Motility

To examine the effects of the *TrpV1* receptor during acupuncture-like stimulation, we next compared optogenetic stimulation (30 mW) with multiple acupuncture-like stimuli in $TrpV1^{ChR2\text{-}eYFP}$ mice, as illustrated in Fig. 4A. Quantitative assessment of colorectal motility parameters (Fig. 4B–F) revealed that both optical stimulation and acupuncture-like interventions elicited significant potentiation of contractile activity, as evidenced by increased AUC and contraction amplitude. The remarkable similarity in re-

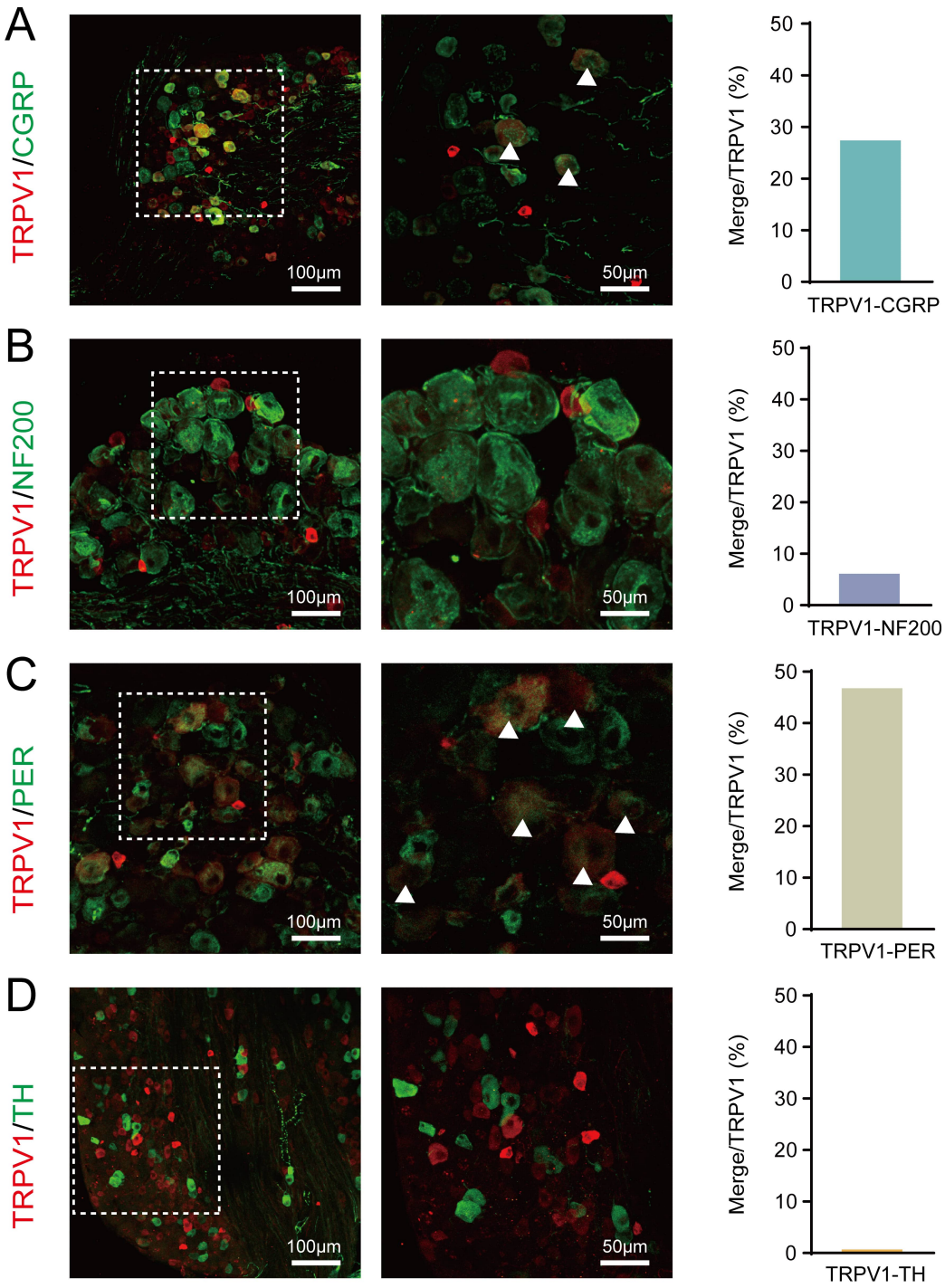

Fig. 2. Molecular characterization of TRPV1^{+} neurons in *TrpV1*^{Cre} mice DRG. (A–D) Representative immunofluorescence images showing the co-expression of TRPV1 (red) with: (A) CGRP (green), (B) NF200 (green), (C) Peripherin (green), and (D) Tyrosine hydroxylase (TH; green). Scale bar: left 100 μm, right 50 μm. Right panels: Quantification of co-localization percentages (mean ± SEM). Arrowheads indicate double stained neurons. TRPV1, transient receptor potential vanilloid 1; DRG, dorsal root ganglion; CGRP, calcitonin gene-related peptide; SEM, Standard error of the mean.

sponse profiles provides compelling evidence that TRPV1-expressing sensory neurons mediate the visceromotor effects of acupuncture-like stimuli.

Quantitative analysis also revealed distinct efficacy profiles among the stimulation modalities (Fig. 5). EA and MA interventions demonstrated superior modulation of colorectal motility function compared to 30 mW optogenetic stimulation (EA: 511.3 ± 125.9% *vs.* 30 mW blue light: 171.6 ± 57.84% of baseline AUC, $p = 0.0423$; EA: 454.9 ± 105.5% *vs.* 30 mW blue light: 179.3 ± 62.46% of base-

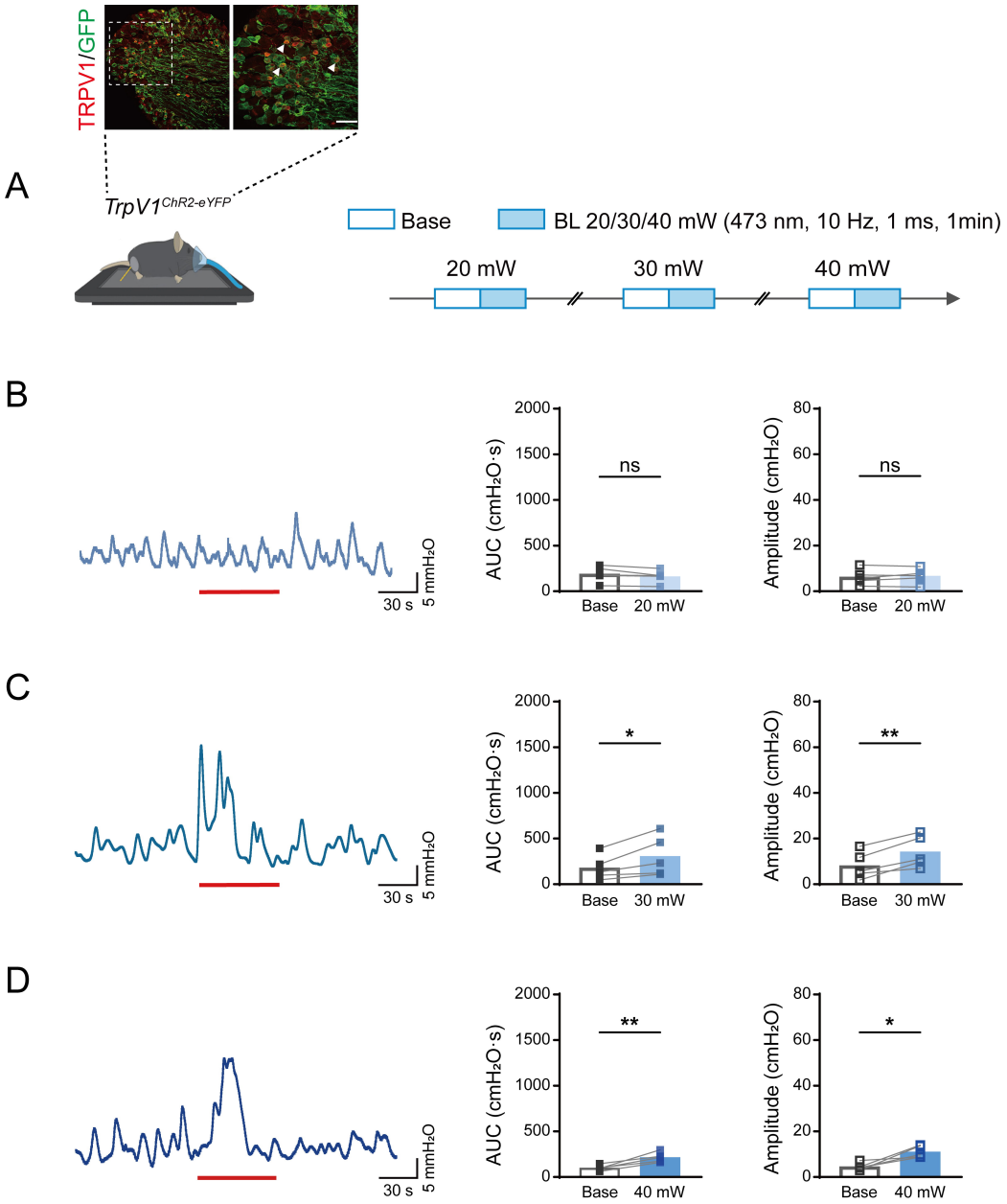

Fig. 3. Effects of different intensities of blue light stimulation at ST36 on colorectal motility in *TrpV1*$^{ChR2\text{-}eYFP}$ mice. (A) Immunofluorescent visualization of *TrpV1*$^{ChR2\text{-}eYFP}$ DRG neurons, showing the expression of ChR2/eYFP (green) and TRPV1 (red) (top). Scale bar, 50 µm. Experimental flowchart for different intensities of blue light stimulation at ST36 in *TrpV1*$^{ChR2\text{-}eYFP}$ mice (bottom). Arrowheads indicate double stained neurons. Mouse image was modified from Heaster TM *et al.* (https://doi.org/10.3389/fbioe.2021.644648). (B–D) Representative example graphs of colorectal motility (left), and statistical graphs of AUC (middle) and amplitude (right) during 20 mW (B), 30 mW (C), and 40 mW (D) blue light stimulation in *TrpV1*$^{ChR2\text{-}eYFP}$ mice at ST36. Length of each red trace refers to 1 min. n = 5, *$p < 0.05$, **$p < 0.01$; ns, not significant, *vs.* base.

line contraction amplitude, $p = 0.0327$; MA: 598.1 ± 136% *vs.* 30 mW blue light: 171.6 ± 57.84% of baseline AUC, $p = 0.008$; MA: 444.6 ± 93.95% *vs.* 30 mW blue light: 179.3 ± 62.46% of baseline contraction amplitude, $p = 0.0415$). In contrast, comparable efficacy profiles were observed for thermal stimulation at 46 °C (144.3 ± 30.71% of baseline AUC, $p = 0.9985$; 155.4 ± 18.98 of baseline contraction amplitude, $p = 0.9976$) and for capsaicin application (189 ± 55.34% of baseline AUC, $p = 0.9998$; 175.4 ± 32.43 of baseline contraction amplitude, $p > 0.9999$), with no significant differences observed between these two modalities.

3.5 Effect of Yellow Light Stimulation at ST36 on Colorectal Motility in TrpV1$^{NpHR\text{-}eYFP}$ *Mice*

We next employed an optogenetic loss-of-function strategy to investigate the contribution of TRPV1^{+} sen-

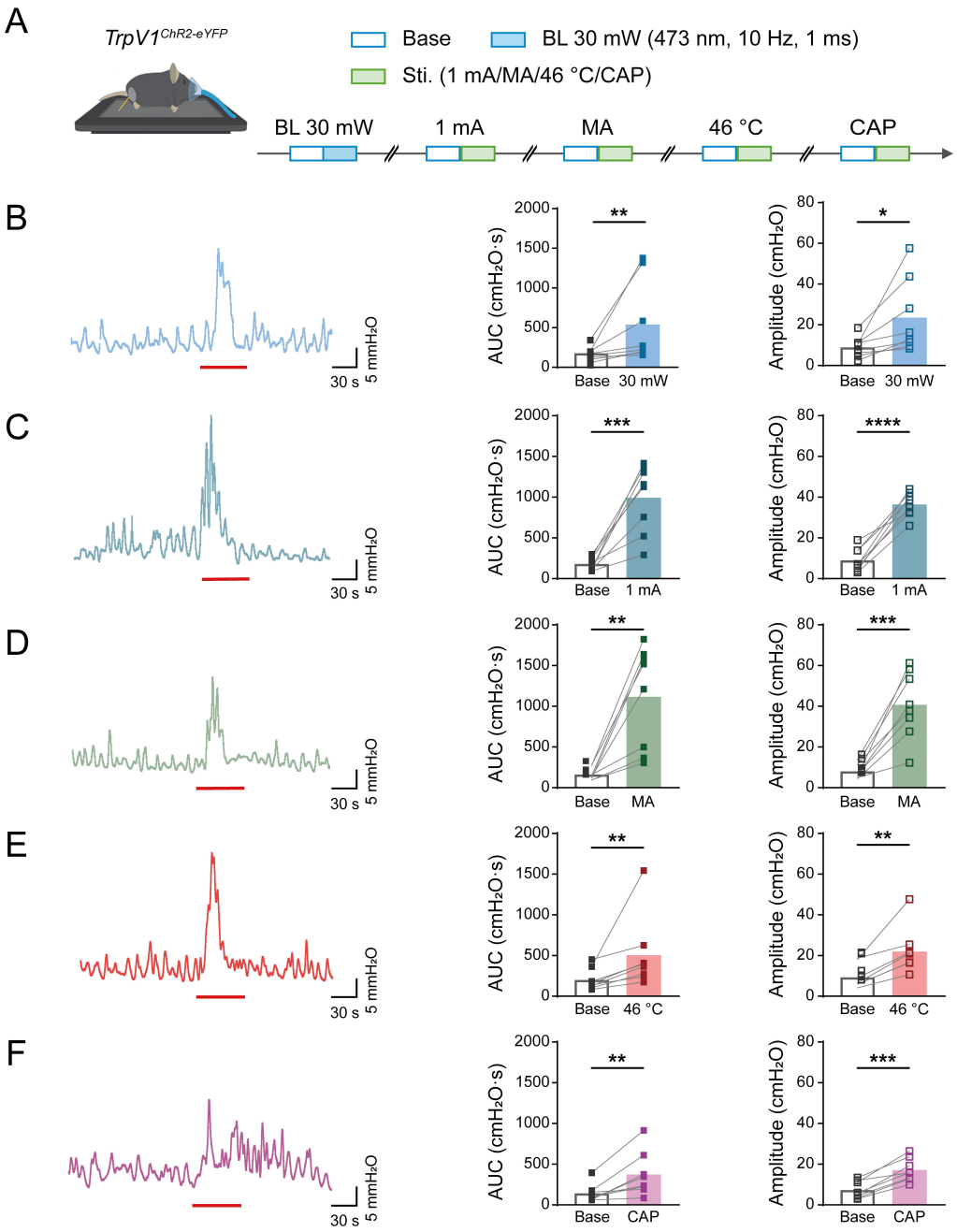

Fig. 4. Colorectal motility of *TrpV1*$^{ChR2\text{-}eYFP}$ mice in response to different acupuncture-like stimuli at ST36. (A) Experimental flowchart for different intensities of blue light stimulation at ST36 in *TrpV1*$^{ChR2\text{-}eYFP}$ mice. Mouse image was modified from Heaster TM *et al.* (https://doi.org/10.3389/fbioe.2021.644648). (B–F) Representative example graphs of colorectal motility (left), and statistical graphs of AUC (middle) and amplitude (right) during stimulation of *TrpV1*$^{ChR2\text{-}eYFP}$ mice at ST36 with 30 mW blue light (B), EA (C), MA (D), 46 °C heat (E), and CAP (F). Length of each red trace refers to 1 min. n = 8, *$p < 0.05$, **$p < 0.01$, ***$p < 0.001$, ****$p < 0.001$ *vs*. base.

sory pathways to acupuncture-evoked colorectal modulation. *TrpV1*$^{NpHR\text{-}eYFP}$ enables cell-type-specific silencing of TRPV1^{+} afferents through yellow light (593 nm) activation of halorhodopsin. Immunohistochemical analysis of DRG sections (L6–S2) revealed precise co-localization of eNpHR3.0-eYFP expression with endogenous TRPV1 immunoreactivity, as shown in Fig. 6A.

To establish the optimal parameters for optogenetic inhibition, we systematically characterized the ideal intensity for yellow light (593 nm) stimulation of colorectal motility in *TrpV1*$^{NpHR\text{-}eYFP}$ mice. As shown in Fig. 6B–D, quantitative analysis revealed that both 30 mW and 40 mW irradiance levels significantly suppressed colorectal motility function. This was evidenced by reduced AUC (30 mW:

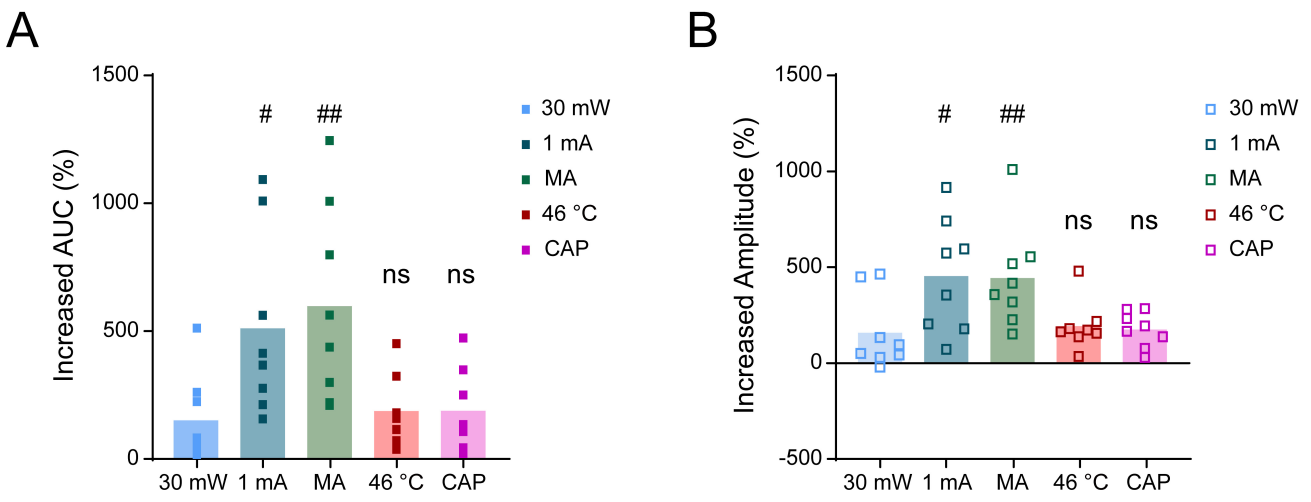

Fig. 5. The extent of increased colorectal motility in *TrpV1*$^{ChR2\text{-}eYFP}$ mice induced by different acupuncture-like stimuli at ST36. (A) Proportion of increase in the AUC of colorectal motility in *TrpV1*$^{ChR2\text{-}eYFP}$ mice during stimulation at ST36 with blue light at 30 mW, EA, MA, 46 °C, and CAP, compared with the respective baselines. (B) Proportion of increase in the amplitude of colorectal motility in *TrpV1*$^{ChR2\text{-}eYFP}$ mice during stimulation at ST36 with blue light at 30 mW, EA, MA, 46 °C, and CAP, compared with the respective baselines. n = 8, $^{\#}p < 0.05$, $^{\#\#}p < 0.01$; ns, not significant, *vs.* 30 mW.

from 471 ± 91.24 to 105.8 ± 19.49 of baseline AUC, p = 0.0207; 40 mW: from 646.8 ± 153.8 to 109.7 ± 31.55, p = 0.0068) and contraction amplitude (30 mW: from 486.5 ± 103 to 160.9 ± 37.94, p = 0.0228; 40 mW: from 609.3 ± 95.84 to 205.3 ± 118.3, p = 0.0064). While the 20 mW irradiance level also reduced contraction amplitude, the change in colorectal motility AUC did not reach statistical significance (20 mW: from 351.6 ± 83.01 to 145.4 ± 28.65 of baseline AUC, p = 0.062; 20 mW: from 349.1 ± 47.91 to 183 ± 34.49 of baseline contraction amplitude, p = 0.0234). Based on comparable efficacy and reduced risk of tissue heating, 30 mW was selected as the standard inhibition parameter in subsequent experiments.

3.6 Opto-Inhibition of TrpV1^{+} Fibers Reduces Acupuncture-Like Effects on Colorectal Motility

To further illustrate the inhibitory effect of TrpV1 during yellow light stimulation, we combined optogenetic inhibition with four distinct somatic acupuncture-like interventions in *TrpV1*$^{NpHR\text{-}eYFP}$ mice (Fig. 7A). Detailed experimental procedures are described in the Methods section. As shown schematically in Fig. 7B–E and Fig. 8A,B, quantitative analysis demonstrated that optogenetic silencing of TRPV1^{+} afferents produced modality-specific attenuation of colorectal motility parameters. For AUC measurements, significant reductions in efficacy were observed across all stimulation conditions, as shown in Fig. 7 (EA: from 695.1 ± 136.4 to 274.3 ± 83.31, p = 0.0408; MA: from 518.4 ± 144.9 to 146 ± 15.32, p = 0.0479; 46 °C: from 347.8 ± 108.7 to 68.04 ± 15.3, p = 0.0464; CAP: from 683.6 ± 218.2 to 102.2 ± 32.57, p = 0.0434). Similarly, analysis of contraction amplitude revealed comparable inhibition profiles (EA: from 717.7 ± 113.6 to 279 ± 96.94, p = 0.0102; MA: from 585.4 ± 136 to 132.9 ± 51.05, p = 0.0407; 46 °C: from 400.9 ± 127.2 to 108.5 ± 31.66, p = 0.0431; CAP: from 856.5 ± 278.7 to 343.1 ± 248.8, p = 0.0196). These findings establish TRPV1^{+} sensory fibers as a critical neural substrate for somatic acupuncture stimulation-induced visceral modulation.

Further analysis revealed that TRPV1-expressing fibers at ST36 differentially mediate the effects of acupuncture-like stimuli modalities on colorectal motor parameters. EA: 64.97 ± 15.26% in AUC, 67.96 ± 13.55% in contraction amplitude; MA: 64.69 ± 7.11% in AUC, 71.09 ± 10.92% in contraction amplitude; 46 °C heat: 77.58 ± 3.89% in AUC, 64.49 ± 6.81% in contraction amplitude; CAP application: 81.95 ± 4.06% in AUC, 69.75 ± 11.43% in contraction amplitude.

4. Discussion

The two key questions addressed in this study were: (1) whether TRPV1 mediated the modulation of colorectal motility by heterogeneous acupoint stimulation, and (2) what the relative contribution of TRPV1 signaling was to these neuromodulatory effects. We functionally dissected these mechanisms by characterizing colorectal motor patterns in genetically distinct mouse strains in response to region-specific light modulation of TRPV1-expressing afferents at the ST36 acupoint.

4.1 Stimulus Paradigm and TPRV1 Characterization

Building on established neurophysiological principles in which Aδ/C-fiber co-activation enhances gastrointestinal motility [13,18], we first verified that diverse somatosensory stimuli (EA, manual acupuncture, 46 °C heat, and cap-

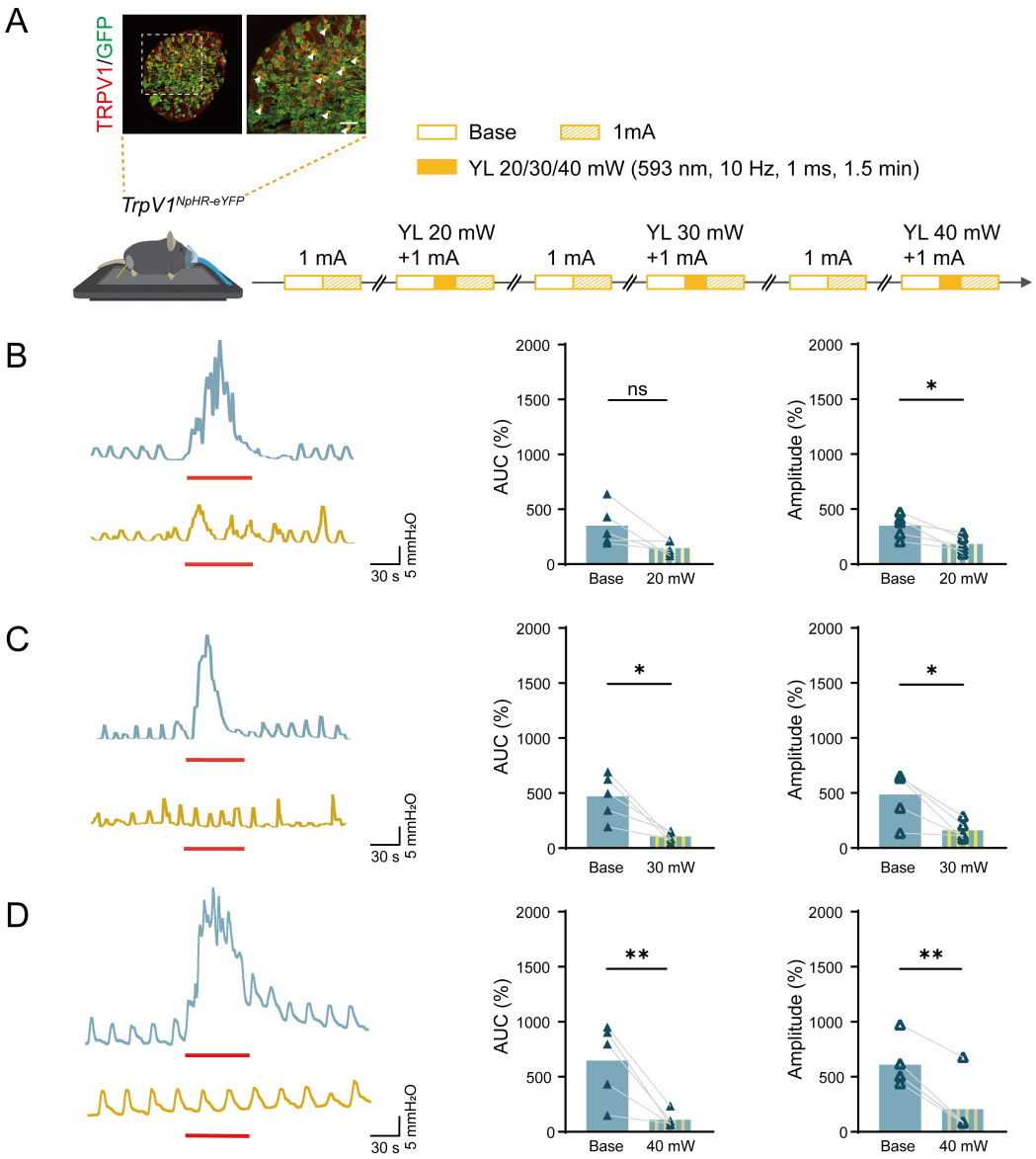

Fig. 6. Effects of EA and EA with different intensities of yellow light stimulation at ST36 on colorectal motility in *TrpV1*$^{NpHR\text{-}eYFP}$ mice. (A) Immunofluorescent visualization of *TrpV1*$^{NpHR\text{-}eYFP}$ DRG neurons showing the expression of NpHR/eYFP (green) and TRPV1 (red) (top). Scale bar, 50 μm. Experimental flowchart for different intensities of yellow light stimulation of ST36 in *TrpV1*$^{NpHR\text{-}eYFP}$ mice (bottom). Arrowheads indicate double stained neurons. Mouse image was modified from Heaster TM *et al.* (https://doi.org/10.3389/fbioe.2021.644648). (B–D) Representative example graphs of colorectal motility (left) and statistical graphs of AUC (middle) and amplitude (right) during EA stimulation and EA with 20 mW (B), 30 mW (C) and 40 mW (D) of yellow light stimulation at ST36 in *TrpV1*$^{NpHR\text{-}eYFP}$ mice. Length of each red trace refers to 1 min. n = 5, *$p < 0.05$, **$p < 0.01$ *vs.* EA; ns, not significant *vs.* EA.

saicin) at ST36 uniformly enhanced colorectal contractile activity in C57BL/6 mice.

TRPV1 serves as a polymodal transducer essential for peripheral nociception, and is therefore predominantly expressed in small- and middle-diameter peripheral neurons [19,20]. Research has shown that its expression is enriched in acupoints and can be dynamically upregulated by EA [19]. In our model, TRPV1 showed preferential co-expression with CGRP^{+} nociceptors (20–25% overlap), but minimal co-localization with NF200^{+} neurons (<6%), indicating predominant association with unmyelinated/thinly myelinated afferents [21]. Further immunohistochemical characterization demonstrates that peripherin (a peripheral neuron marker) colocalizes with TRPV1 in ~50% of small/medium neurons, confirming predominant peripheral nociceptor expression. Tyrosine hydroxylase (TH), a marker for C-fiber low-threshold mechanoreceptors (on average, 15% of mouse DRG neurons express TH) [22], shows no co-expression with TRPV1. Collectively, these findings establish TRPV1 as a selective biomarker

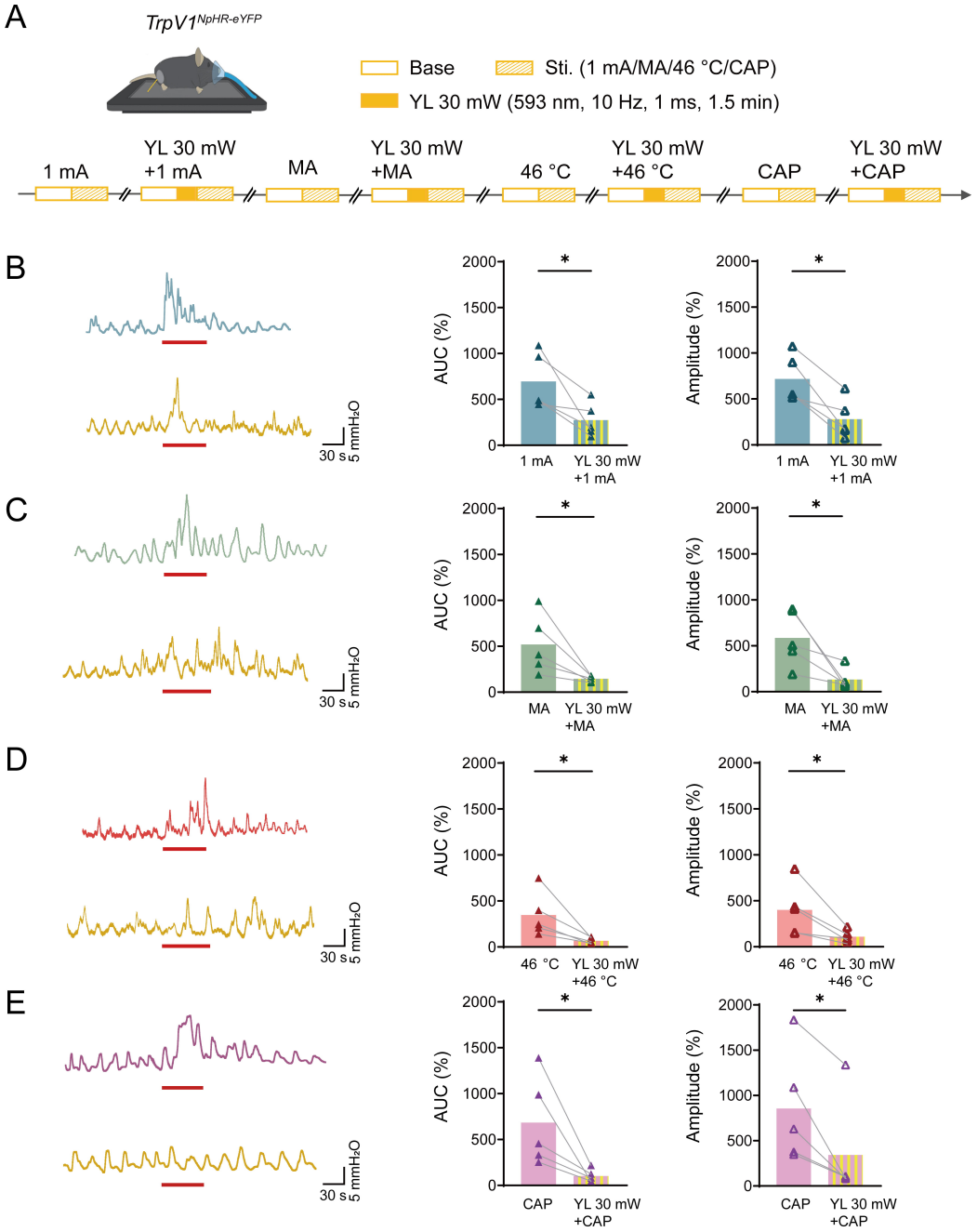

Fig. 7. Effects of acupuncture-like stimuli and acupuncture-like stimuli combined with yellow light stimulation at ST36 on colorectal motility in *TrpV1*$^{NpHR\text{-}eYFP}$ mice. (A) Experimental flowchart for four different stimuli and stimuli with 30 mW yellow light stimulation at ST36 in *TrpV1*$^{NpHR\text{-}eYFP}$ mice. Mouse image was modified from Heaster TM *et al.* (https://doi.org/10.3389/fbioe.2021.644648). (B–E) Representative example graphs of colorectal motility (left), and statistical graphs of AUC (middle) and amplitude (right) of acupuncture-like stimuli: EA (B), MA (C), 46 °C heat (D), and CAP (E), and acupuncture-like stimuli with 30 mW yellow light stimulation in *TrpV1*$^{NpHR\text{-}eYFP}$ mice at ST36. Length of each red trace refers to 1 min. n = 5, *$p < 0.05$ *vs.* sti.

for small-to-medium diameter nociceptive neurons in somatosensory pathways.

4.2 In Vivo Optogenetic Activation and Inhibition

Specific optogenetic activation of TRPV1^{+} afferents with blue light (473 nm) enhanced colorectal motility in *TrpV1*$^{ChR2\text{-}eYFP}$ mice. The effect was comparable in amplitude to that induced by 46 °C heat or capsaicin interventions, but was less potent than EA or MA (Fig. 5). This mechanistic divergence arises from differential nociceptor engagement profiles, with 46 °C heat, capsaicin and optogenetic stimulation primarily activating cutaneous TRPV1^{+} fibers, whereas EA and MA concurrently engage multiple nociceptor subtypes (e.g., TRPV1^{+}, ASIC3^{+},

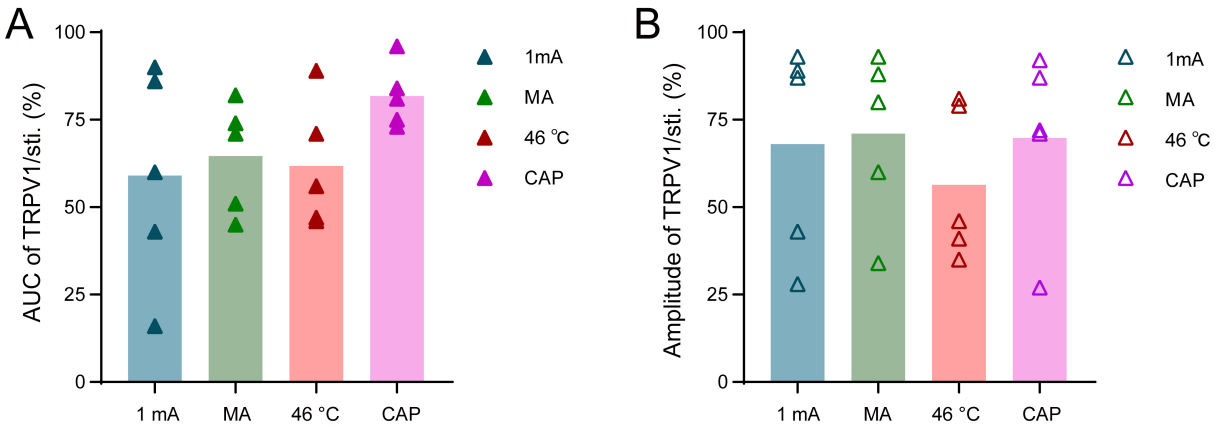

Fig. 8. The proportion of contribution of TRPV1 to the facilitation of colorectal motility under various acupuncture-like stimuli at ST36. (A) Statistical chart of the proportion of TRPV1's effect on the AUC of colorectal motility in *TrpV1*$^{NpHR\text{-}eYFP}$ mice induced by EA, MA, 46 °C heat, and CAP stimulation at ST36. (B) Statistical chart of the proportional effect of TRPV1 on the amplitude of colorectal motility in *TrpV1*$^{NpHR\text{-}eYFP}$ mice induced by EA, MA, 46 °C heat, and CAP stimulation at ST36. n = 5.

P2X3$^+$ populations) across cutaneous and muscular compartments, generating synergistic neuromodulatory effects through spatial summation in spinal cord projection neurons [23].

Conversely, optogenetic inhibition of TRPV1$^+$ afferents during EA at ST36 with yellow light (589 nm) in *TrpV1*$^{NpHR\text{-}eYFP}$ mice significantly attenuated the stimulation-induced potentiation of colorectal motility by various modalities (Figs. 6,7). Consistent with previous findings in TRPV1 KO mice, our results support the crucial role of TRPV1 in mediating acupuncture-like stimuli effects [24]. Notably, Dong *et al.* [25] recently provided direct functional evidence by demonstrating that specific pharmacological inhibition of deep TRPV1$^+$ sensory fibers innervating the ST36 region prevented EA at ST36 from effectively triggering gastric reflexes. This finding suggests that deep TRPV1$^+$ sensory fibers innervating the ST36 fascial compartment are one of the key initial components in the cascade of EA-promoted gastric motility [25]. As shown in Fig. 8, we observed variations in the relative contribution of TRPV1-mediated signaling to colorectal motility regulation depending on the stimulus. This indicates that TRPV1 plays a complex role in mediating the regulatory effects of acupuncture-like stimuli on colorectal motility, with variable contributions depending on the type of stimulation and the specific metrics measured. While optogenetic silencing of TRPV1$^+$ fibers at the ST36 acupoint was utilized in this study, future validation should incorporate orthogonal approaches. This could include topical application of selective antagonists, and chemogenetic inhibition via DREADD-expressing models to establish modality-independent causality.

4.3 Involvement of Downstream Neural Pathways

A key consideration is how activation of TRPV1$^+$ afferents in the hindlimb (ST36) influences distant visceral motility. The somato-visceral pathway recruited by ST36 stimulation likely involves both spinal and vagal mechanisms. Afferents from the ST36 region (tibialis anterior muscle) primarily originate from lumbar DRGs (L4–L6) and project to the corresponding spinal segments [26]. Following initial integration in the spinal cord, this information may influence colorectal motility via a spino-bulbo-vagal pathway [24], reaching brainstem nuclei such as the nucleus tractus solitarius and the dorsal motor nucleus of the vagus, ultimately modulating gastrointestinal function through vagal efferents. Supporting vagal involvement, optogenetic stimulation of ST36 has been shown to robustly potentiate cervical vagal efferent activity. Thus, the observed modulation of colorectal motility may result from activation of TRPV1$^+$ lumbar afferents at ST36 and their subsequent integration within this spino-vagal axis.

4.4 Limitations and Future Perspectives

While optogenetics provides cell-type-specific causality, several limitations should be considered. (1) The penetration depth of transdermal optical stimulation is limited, likely affecting cutaneous and superficial subcutaneous fibers [27,28]. (2) Experiments were conducted under isoflurane anesthesia, which may influence autonomic tone and baseline colonic motility [29]. (3) While our motility data support effective inhibition by yellow light, we lack *in vivo* electrophysiological recordings (e.g., from the sciatic nerve or dorsal roots) to directly quantify the silencing efficiency of TRPV1$^+$ fibers during NpHR activation. (4) Sample sizes were small for some experimental groups. Future studies should employ orthogonal approaches—such as topical application of selective antagonists and chemogenetic inhibition—for validation, and directly investigate the complete neural circuitry in awake, behaving models.

5. Conclusions

Our research has provided novel insights into the regulatory role of TRPV1 receptors in colorectal motility when activated in an acupoint-targeted manner, with the elucidation of key mechanisms in this physiological process. This enhances our understanding of the role of TRPV1 in regulating gastrointestinal function, as well as having significant implications for clinical practice. Specifically, by considering the degree of TRPV1 involvement as a key biomarker, we anticipate substantial improvements in the design of therapeutic interventions, leading to more effective improvement of neuroregulatory functions in the gastrointestinal tract. The present work establishes a theoretical basis for developing novel therapeutic strategies to address common conditions such as functional gastrointestinal disorders, ultimately improving clinical outcomes and patient quality of life.

Abbreviations

FGIDs, Functional gastrointestinal disorders; DRG, Dorsal root ganglion; ST36, Zusanli acupoint; EA, Electroacupuncture; MA, Manual acupuncture; AUC, Area under the curve; TH, Tyrosine hydroxylase; RCTs, Randomized clinical trials; TRPV1, Transient receptor potential vanilloid 1; OCT, Optimal cutting temperature; SEM, Standard error of the mean; ANOVA, Analysis of variance.

Availability of Data and Materials

Data will be made available upon request from the corresponding author.

Author Contributions

NZ: Methodology, Validation, Formal analysis, Investigation, Data curation, Writing—original draft, Writing—review and editing, Supervision, Project administration. HC: Investigation, Writing—review and editing, Visualization. XG: Conceptualization, Investigation, Resources, Supervision, Project administration. SL: Methodology, Formal analysis, Investigation, Data curation. WL: Methodology, Formal analysis, Investigation. XL: Validation, Formal analysis, Investigation. KL: Validation, Formal analysis, Investigation. SW: Conceptualization, Resources, Supervision, Project administration, Funding acquisition. BZ: Conceptualization, Resources, Supervision, Project administration, Funding acquisition. All authors contributed to editorial changes in the manuscript. All authors read and approved the final manuscript for publication. All authors have participated sufficiently in the work and agreed to be accountable for all aspects of the work.

Ethics Approval and Consent to Participate

All experimental procedures were conducted in accordance with the National Institutes of Health Guide for the Care and Use of Laboratory Animals and were approved by the Experimental Animal Ethics Committee of the China Academy of Chinese Medical Sciences (No. D2024-01-26-07).

Acknowledgment

Not applicable.

Funding

This study was supported by National Natural Science Foundation of China (82230123, 82174281), and the Fundamental Research Funds for the Central Public Welfare Research Institutes (ZZ14-YQ-033).

Conflict of Interest

The authors declare no conflict of interest.

References

[1] Liu Z, Yan S, Wu J, He L, Li N, Dong G, *et al*. Acupuncture for Chronic Severe Functional Constipation: A Randomized Trial. Annals of Internal Medicine. 2016; 165: 761–769. https://doi.org/10.7326/M15-3118.

[2] Yang JW, Wang LQ, Zou X, Yan SY, Wang Y, Zhao JJ, *et al*. Effect of Acupuncture for Postprandial Distress Syndrome: A Randomized Clinical Trial. Annals of Internal Medicine. 2020; 172: 777–785. https://doi.org/10.7326/M19-2880.

[3] Pei L, Geng H, Guo J, Yang G, Wang L, Shen R, *et al*. Effect of Acupuncture in Patients With Irritable Bowel Syndrome: A Randomized Controlled Trial. Mayo Clinic Proceedings. 2020; 95: 1671–1683. https://doi.org/10.1016/j.mayocp.2020.01.042.

[4] Wang Y, Yang JW, Yan SY, Lu Y, Han JG, Pei W, *et al*. Electroacupuncture vs Sham Electroacupuncture in the Treatment of Postoperative Ileus After Laparoscopic Surgery for Colorectal Cancer: A Multicenter, Randomized Clinical Trial. JAMA Surgery. 2023; 158: 20–27. https://doi.org/10.1001/jamasurg.2022.5674.

[5] Pei L, Wang G, Yang S, Zhou S, Xu T, Zhou J, *et al*. Electroacupuncture Reduces Duration of Postoperative Ileus After Laparoscopic Gastrectomy for Gastric Cancer: A Multicenter Randomized Trial. Gastroenterology. 2025; 169: 73–84. https://doi.org/10.1053/j.gastro.2025.02.006.

[6] Xu GY, Winston JH, Chen JDZ. Electroacupuncture attenuates visceral hyperalgesia and inhibits the enhanced excitability of colon specific sensory neurons in a rat model of irritable bowel syndrome. Neurogastroenterology and Motility. 2009; 21: 1302-e125. https://doi.org/10.1111/j.1365-2982.2009.01354.x.

[7] Song J, Yin J, Sallam HS, Bai T, Chen Y, Chen JDZ. Electroacupuncture improves burn-induced impairment in gastric motility mediated via the vagal mechanism in rats. Neurogastroenterology and Motility. 2013; 25: 807-e635. https://doi.org/10.1111/nmo.12183.

[8] Zhang B, Hu Y, Shi X, Li W, Zeng X, Liu F, *et al*. Integrative Effects and Vagal Mechanisms of Transcutaneous Electrical Acustimulation on Gastroesophageal Motility in Patients With Gastroesophageal Reflux Disease. The American Journal of Gastroenterology. 2021; 116: 1495–1505. https://doi.org/10.14309/ajg.0000000000001203.

[9] Xi H, Li X, Zhang Z, Cui X, Zhu B, Jing X, *et al*. Continuous peripheral electrical nerve stimulation improves cardiac function via autonomic nerve regulation in MI rats. Heart Rhythm. 2024; 21: 2010–2019. https://doi.org/10.1016/j.hrthm.2024.04.070.

[10] Meltzer S, Santiago C, Sharma N, Ginty DD. The cellular and molecular basis of somatosensory neuron development. Neuron.

2021; 109: 3736–3757. https://doi.org/10.1016/j.neuron.2021.09.004.

[11] Basbaum AI, Bautista DM, Scherrer G, Julius D. Cellular and molecular mechanisms of pain. Cell. 2009; 139: 267–284. https://doi.org/10.1016/j.cell.2009.09.028.

[12] Caterina MJ, Schumacher MA, Tominaga M, Rosen TA, Levine JD, Julius D. The capsaicin receptor: a heat-activated ion channel in the pain pathway. Nature. 1997; 389: 816–824. https://doi.org/10.1038/39807.

[13] Su YS, Xin JJ, Yang ZK, He W, Shi H, Wang XY, *et al*. Effects of Different Local Moxibustion-Like Stimuli at Zusanli (ST36) and Zhongwan (CV12) on Gastric Motility and Its Underlying Receptor Mechanism. Evidence-based Complementary and Alternative Medicine: ECAM. 2015; 2015: 486963. https://doi.org/10.1155/2015/486963.

[14] Yu Z, Zhang N, Lu CX, Pang TT, Wang KY, Jiang JF, *et al*. Electroacupuncture at ST25 inhibits jejunal motility: Role of sympathetic pathways and TRPV1. World Journal of Gastroenterology. 2016; 22: 1834–1843. https://doi.org/10.3748/wjg.v22.i5.1834.

[15] Makadia PA, Najjar SA, Saloman JL, Adelman P, Feng B, Margiotta JF, *et al*. Optogenetic Activation of Colon Epithelium of the Mouse Produces High-Frequency Bursting in Extrinsic Colon Afferents and Engages Visceromotor Responses. The Journal of Neuroscience. 2018; 38: 5788–5798. https://doi.org/10.1523/JNEUROSCI.0837-18.2018.

[16] Madisen L, Mao T, Koch H, Zhuo JM, Berenyi A, Fujisawa S, *et al*. A toolbox of Cre-dependent optogenetic transgenic mice for light-induced activation and silencing. Nature Neuroscience. 2012; 15: 793–802. https://doi.org/10.1038/nn.3078.

[17] Cavanaugh DJ, Chesler AT, Jackson AC, Sigal YM, Yamanaka H, Grant R, *et al*. Trpv1 reporter mice reveal highly restricted brain distribution and functional expression in arteriolar smooth muscle cells. The Journal of Neuroscience. 2011; 31: 5067–5077. https://doi.org/10.1523/JNEUROSCI.6451-10.2011.

[18] Tominaga M, Caterina MJ, Malmberg AB, Rosen TA, Gilbert H, Skinner K, *et al*. The cloned capsaicin receptor integrates multiple pain-producing stimuli. Neuron. 1998; 21: 531–543. https://doi.org/10.1016/s0896-6273(00)80564-4.

[19] Abraham TS, Chen ML, Ma SX. TRPV1 expression in acupuncture points: response to electroacupuncture stimulation. Journal of Chemical Neuroanatomy. 2011; 41: 129–136. https://doi.org/10.1016/j.jchemneu.2011.01.001.

[20] Gou Q, Song Z, Gong Y, Li J. TRPV1 in Dry Eye Disease. Frontiers in Bioscience (Landmark Edition). 2024; 29: 175. https://doi.org/10.31083/j.fbl2905175.

[21] Cui YY, Xu H, Wu HH, Qi J, Shi J, Li YQ. Spatio-temporal expression and functional involvement of transient receptor potential vanilloid 1 in diabetic mechanical allodynia in rats. PloS One. 2014; 9: e102052. https://doi.org/10.1371/journal.pone.0102052.

[22] Brumovsky PR. Dorsal root ganglion neurons and tyrosine hydroxylase–an intriguing association with implications for sensation and pain. Pain. 2016; 157: 314–320. https://doi.org/10.1097/j.pain.0000000000000381.

[23] Lawson SN, Fang X, Djouhri L. Nociceptor subtypes and their incidence in rat lumbar dorsal root ganglia (DRGs): focussing on C-polymodal nociceptors, Aβ-nociceptors, moderate pressure receptors and their receptive field depths. Current Opinion in Physiology. 2019; 11: 125–146. https://doi.org/10.1016/j.cophys.2019.10.005.

[24] Li YQ, Zhu B, Rong PJ, Ben H, Li YH. Neural mechanism of acupuncture-modulated gastric motility. World Journal of Gastroenterology. 2007; 13: 709–716. https://doi.org/10.3748/wjg.v13.i5.709.

[25] Dong S, Zhao L, Liu J, Sha X, Wu Y, Liu W, *et al*. Neuroanatomical organization of electroacupuncture in modulating gastric function in mice and humans. Neuron. 2025; 113: 3243–3259.e11. https://doi.org/10.1016/j.neuron.2025.06.023.

[26] Lu MJ, Yu Z, He Y, Yin Y, Xu B. Electroacupuncture at ST36 modulates gastric motility *via* vagovagal and sympathetic reflexes in rats. World Journal of Gastroenterology. 2019; 25: 2315–2326. https://doi.org/10.3748/wjg.v25.i19.2315.

[27] Lister T, Wright PA, Chappell PH. Optical properties of human skin. Journal of Biomedical Optics. 2012; 17: 90901–90901. https://doi.org/10.1117/1.JBO.17.9.090901.

[28] Sabino CP, Deana AM, Yoshimura TM, da Silva DFT, França CM, Hamblin MR, *et al*. The optical properties of mouse skin in the visible and near infrared spectral regions. Journal of Photochemistry and Photobiology. B, Biology. 2016; 160: 72–78. https://doi.org/10.1016/j.jphotobiol.2016.03.047.

[29] Dryn D, Luo J, Melnyk M, Zholos A, Hu H. Inhalation anaesthetic isoflurane inhibits the muscarinic cation current and carbachol-induced gastrointestinal smooth muscle contractions. European Journal of Pharmacology. 2018; 820: 39–44. https://doi.org/10.1016/j.ejphar.2017.11.044.